Electron-spectral-line profiles of resonances by attosecond XUV or x-ray pulses

Song Bin Zhang,[1,*] Xiao Tao Xie,[1] and Jian Guo Wang[2]
[1]*School of Physics and Information Technology, Shaanxi Normal University, 710119 Xi'an, China*
[2]*Institute of Applied Physics and Computational Mathematics, P.O. Box 8009, Beijing 100088, China*
(Received 20 July 2017; revised manuscript received 23 September 2017; published 20 November 2017)

An attosecond XUV or x-ray pump-control scheme for the electron-spectral-line profiles of Fano and Auger resonances is proposed and studied. A weak pump resonantly excites the atom and creates the resonance, and then a second strong attosecond control pulse resonantly coupling the resonance to an valance excited state is applied at different time delays (Δt_{21}). Resonance with lifetimes ($1/\Gamma$) much longer than the pulse duration (τ) is studied. It is found that the dynamic variations of the electron spectra can be partitioned into two or three regions with respect to the time delays and pulse area of the control pulse: explicitly, the overlap region ($\Delta t_{21} <\sim 4\tau$) and analysis region ($\Delta t_{21} >\sim 4\tau$) in the case with a sub-π-control pulse; and the overlap region ($\Delta t_{21} <\sim 4\tau$), reverse region ($\sim 4\tau < \Delta t_{21} <\sim 2/\Gamma$), and analysis region ($\Delta t_{21} >\sim 2/\Gamma$) in the case with a sub-2π-control pulse. In the case with a sub-π-control pulse, the electron spectral line profiles do not change too much and only the degrees of asymmetries of the spectra are reduced in the overlap region, while in the analysis region, the main profiles of the electron spectra are maintained but with modulation structures. In the case with a sub-2π-control pulse, the electron spectral line profiles totally reverse the asymmetries in the overlap region, while in the reverse region, the electron spectra keep the reversed asymmetries but with modulation structures, and the electron spectra pertain the modulation structures in the analysis region but with the main profiles reversed. All these dynamic features of the electron spectra can be fully understood with the help of an analytic theory, which is also fully presented based on the time-dependent perturbation theory.

DOI: 10.1103/PhysRevA.96.053420

I. INTRODUCTION

Bound and continuum states are the stationary states of a quantum system, while resonances are known as the discrete quantum states embedded in and coupled to continuums in the time-independent picture, which is introduced by the configuration interactions between the discrete quantum states and the continuums [1–3]. Resonances are not stationary states and occur in quantum collisions as the metastable states of the scattering system. In electron collisions with an N-electron target, a resonance (state) is created if the projectile electron is temporarily captured by the target and compounds with the target into a metastable state of the $(N+1)$-electron scattering system. While in photon scatterings, the target can be excited into metastable states, such as doubly excited states and core hole Auger states of the target, which are also known as resonances. Explicitly, taking a helium atom as an example, the doubly excited state He($2s2p$, $^1P^o$) can be considered as a resonance state in electron collisions with $He^+(1s)$ or a resonance in photon scattering with He($1s^2$). Shape and Feshbach resonances are the mostly employed two classifications of resonances from the interaction-potential picture. The interactions between the projectile electron and the target are represented by different potential curves, and each potential curve is known as a channel. If a potential barrier exists in one channel and is strong enough to temporarily capture the projectile electron, the state of the potential-barrier-captured electron can tunnel decay into the same channel and is known as the Shape resonance. If there are coupled interactions between two channels, a potential well exists in the up channel and is deep enough to capture the projectile electron or they can compound into a discrete state, and the compounded discrete state is also energetically above the limits of the down channel, such kind of discrete state can decay into the down channel as a continuum by the adiabatic channel interactions and is known as the Feshbach resonance or Fano resonance [4–7]. Generally, resonances contribute abrupt changes of the scattering cross sections and play important roles in quantum collision dynamics, so the studies of resonance, including the resonance itself and the methods to study resonance, are important and of long-standing interest in conventional atomic and molecular physics [3–13].

The very recent works [14,15] of Pfeifer's group in Heidelberg in ultrafast control of resonance have opened up a new pathway to study resonance and have brought resonances into the field of ultrafast and strong-field physics. Attosecond XUV pump and femtosecond IR control [Fig. 1(a)] has become into a standard technique to manipulate the spectral line profiles of resonances between the symmetric Lorentzian and asymmetric Fano line shapes [16–29]. When the resonant attosecond XUV-pump laser is on, the electrons are excited in two different pathways: one with the electrons resonantly excited into the resonance state and the other with the electrons directly ionized into the continuum. The electrons in the resonance state simultaneously decay into the same continuum state as in the second pathway. The electrons from two different pathways into the same continuum state ultimately interfere and exhibit the line profiles in the scattering cross sections. Resonance is created by excitation from an initial reference state and its existence is independent of the reference state, while the exhibition of its effects depends on the reference state. Compared to the time-independent picture, the time-dependent picture can present a much more clear picture of the dynamical processes of excitation, decay, and interference of resonance.

*song-bin.zhang@snnu.edu.cn

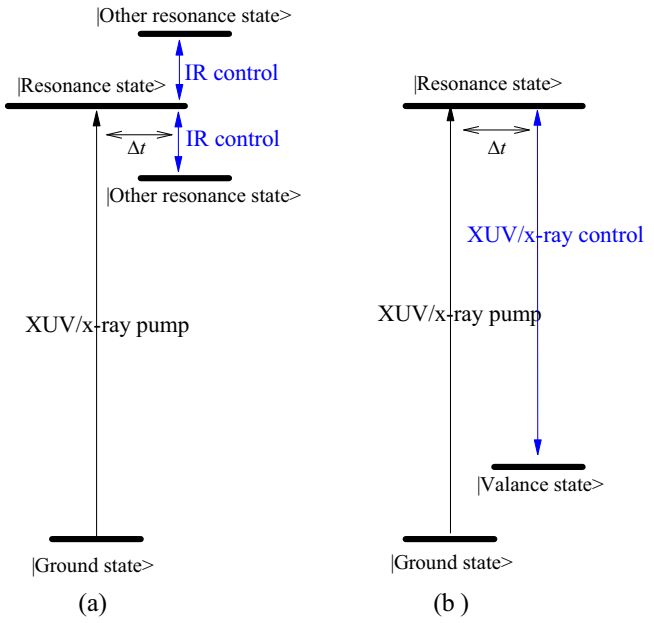

FIG. 1. Schematics of the XUV or x-ray pump and IR control (a), and XUV or x-ray control (b) schemes; the control pulse is time delayed by Δt. Note that the pump pulse resonantly excites the ground state into a resonance state, and the control pulse resonantly couples the resonance state to other resonance states (a) or the valance state (b). Generally, the pump pulse would be an XUV pulse if the resonance state is a lowly excited Fano resonance state, while both pump and control pulses would be x-ray pulses if the resonance state is a highly excited Auger state.

With the strong time-delayed femtosecond IR-control laser, the strong IR pulse could cycle the electrons of the resonance state through some intermediate states back to the resonance state and change the wave-packet dynamics (phase and amplitude) of the resonance state. The inference pattern of the electron spectra from the two pathways would ultimately be changed and even reversed between the symmetric Lorentzian and asymmetric Fano line shapes. Such kind of manipulations can be easily understood from Fano's description of resonance [5–7]. The cross sections at photon energy E is given in terms of Fano factor $q = \frac{\langle D_E|z|0\rangle}{\pi\langle B|H|C_E\rangle\langle C_E|z|0\rangle}$ as [5–7]

$$\sigma(E) = \sigma_a \frac{(q+\eta)^2}{1+\eta^2} + \sigma_b, \tag{1}$$

where $\eta = \frac{E-E_0}{\Gamma/2}$ is the scaled energy difference with E_0 and Γ as the position and width of the resonance, respectively; σ_a and σ_b represent two portions of the cross section corresponding, respectively, to transitions from initial state $|0\rangle$ to states of the continuum $|C_E\rangle$ (normalized to per unit energy) that do and do not interact with the discrete autoionizing state $|B\rangle$; $|D_E\rangle$ is the dressed discrete state produced by the interaction of H with the mixing of the old discrete state $|B\rangle$ and the continuum [30]. The way of changing the wave packet dynamics of the resonance with IR-control pulse approximately equals to change the phase and amplitude of the transition matrix element $\langle D_E|z|0\rangle$ or the Fano factor q. In this way, the profiles of the cross section can be surely manipulated. Note that when q is changed by phase π into $-q$, the profiles of the spectra will be totally reversed, and when $|q|$ is changed from a big number into a small one, the profiles of the spectra will be transferred from the symmetric Lorentzian into asymmetric Fano shape.

The above scheme of attosecond XUV pump and femtosecond IR control is easy to implement and is broadly applied. However, the strong IR pulse can couple to many unknown intermediate states [see Fig. 1(a)] and the pulse duration of the control pulse is not too short compared to the decay lifetime ($1/\Gamma$, tens of femtosecond) of the resonance state, which would introduce significant changes to the results by neglecting the decay during the implementation of the control pulse. These create great difficulties when analyzing the results and make the manipulation unpredictable. In this work, we present an attosecond XUV or x-ray pump-control scheme [see Fig. 1(b)] for the manipulation of the electron spectral line profiles of Fano and Auger resonances. Explicitly, a weak pump resonantly excites the atom and creates the resonance, and then a strong attosecond control pulse resonantly coupling the resonance to an valance excited state is applied at different time delays (Δt_{21}). Since generally the present pulses are much shorter than the lifetime of the resonance state, the manipulation of the resonance state can be fully understood with the help of an analytic theory, which is also fully presented based on the time-dependent perturbation theory. It is found that the dynamic variations of the electron spectra can be partitioned into different regions with respect to the time delay, and the attosecond x-ray control pulse can be even applied to instantly terminate the wave packet dynamics of the resonance state with properly selected pulse parameters. At the same time, the instant information of the wave packet is mapped onto the electron spectra (see Sec. III for details). Bearing in mind that because the techniques of creating multicolor x rays at present-day x-ray free-electron laser facilities (FELs) of different wavelengths, pulse durations, and relative time delays are rapidly evolving [31–33], several schemes have been proposed to produce transform-limited attosecond and femtosecond pulses [34–37], and the present attosecond XUV or x-ray pump-control scheme should be feasible in future FEL facilities. This work presents a pathway for the applications of attosecond x-ray FELs. At rest, the typical resonance state or doubly excited state He($2s2p$, $^1P^o$) is taken as an example to fully show the present pump-control scheme. Unless otherwise stated, atomic units (a.u.) are used throughout the paper.

II. THEORETICAL METHOD

The time-dependent wave-packet-propagation method [38–42] is employed to evaluate the dynamics of the electronic states and the electron spectra. The total wave function $\Psi(t)$ can be formally expanded with the complete basis $\{|b\rangle, |\kappa\rangle\}$ of the field-free Hamiltonian as

$$\Psi(t) = \sum_b a_b(t)|b\rangle + \int a_\kappa(t)|\kappa\rangle d\kappa, \tag{2}$$

where $\{a_b(t)\}$ and $\{a_\kappa(t)\}$ are the corresponding time-dependent expansion coefficients for the discrete bound basis $|b\rangle$ and continuum basis $|\kappa\rangle$, respectively. Bearing in mind that high-frequency XUV or x-ray laser pulses are employed to drive the system, the formal expansion of Eq. (2) can be

reasonably and greatly simplified by approximately taking into account the resonantly excited states by the lasers. Explicitly, for the present study of doubly excited state He($2s2p$, $^1P^o$) by pump and control lasers with frequencies ω_1 and ω_2, respectively, the total wave function can be well described as

$$\Psi(t) = a_{1s^2}(t)|1s^2\rangle + \int d\varepsilon a_{1s\varepsilon p}(\varepsilon,t)e^{-i\omega_1 t}|1s\varepsilon p\rangle + a_{2s2p}(t)e^{-i\omega_1 t}|2s2p\rangle + a_{1s2s}e^{-i(\omega_1-\omega_2)t}|1s2s\rangle, \quad (3)$$

where $a_{1s^2}(t)$, $a_{2s2p}(t)$, $a_{1s2s}(t)$, and $a_{1s\varepsilon p}(\varepsilon,t)$ are the time-dependent amplitudes of the bound levels $|1s^2\rangle$, $|2s2p\rangle$, $|1s2s\rangle$, and continuum level $|1s\varepsilon p\rangle$, respectively. The rapid evolving phase factors $e^{-i\omega_1 t}$ and $e^{-i(\omega_1-\omega_2)t}$ are explicitly separated. After inserting $\Psi(t)$ into the time-dependent Schrödinger equation for the total Hamiltonian and applying the rotating-wave approximation [43,44] and the local approximation [38,45,46], the following working equations for the expansion coefficients with a specific electron energy ε can be proposed:

$$i\dot{\Phi}(\varepsilon,t) = \bar{\mathbf{H}}(\varepsilon,t)\Phi(\varepsilon,t), \quad (4)$$

where

$$\Phi(\varepsilon,t) = [a_{1s^2}(t), a_{2s2p}(t), a_{1s\varepsilon p}(\varepsilon,t), a_{1s2s}(t)]^{\mathrm{T}} \quad (5)$$

and

$$\bar{\mathbf{H}}(\varepsilon,t) = \begin{bmatrix} E_{1s^2} - \frac{i}{2}\Gamma_{\mathrm{ph}}(t) & D_{12}^{\dagger}(t_1,t) & 0 & 0 \\ D_{12}(t_1,t) & E_{2s2p} - \frac{i}{2}\Gamma - \omega_1 & 0 & D_{24}^{\dagger}(t_2,t) \\ D_{13}(t_1,t) & V & E_{1s} + \varepsilon - \omega_1 & 0 \\ 0 & D_{24}(t_2,t) & 0 & E_{1s2s} + \omega_2 - \omega_1 \end{bmatrix}. \quad (6)$$

E_i is the level energy for state $|i\rangle$, $\Gamma = 2\pi|V|^2$ is the decay width of the resonance, and $\Gamma_{\mathrm{ph}}(t) = 2\pi|D_{13}(t)|^2$ indicates the leakage of the ground state by direct photoionization. The dipole coupling term $D_{ij}(t_i,t) = \frac{\Omega_{ij}}{2}g(t_i,t) = \frac{d_{ij}g_0}{2}g(t_i,t)$, where g_0, $d_{ij} = \langle j|z|i\rangle$ and Ω_{ij} are the pulse electric intensity, transition dipole moment, and Rabi frequency between states $|i\rangle$ and $|j\rangle$, respectively. The Gaussian pulse $g(t_i,t) = e^{-4\ln 2\frac{(t_i-t)^2}{\tau^2}}$ is employed, t_i is the pulse center far from time zero, and the resonant frequencies for the pump and control pulses are $\omega_1 = E_{2s2p} - E_{1s^2}$ and $\omega_2 = E_{2s2p} - E_{1s2s}$, respectively. The electron spectrum $\sigma_{He^+(1s)}(\varepsilon)$ pertaining to the ionic state $He^+(1s)$ is given by

$$\sigma_{He^+(1s)}(\varepsilon) = \lim_{t\to\infty}\langle a_{1s\varepsilon p}(\varepsilon,t)|a_{1s\varepsilon p}(\varepsilon,t)\rangle. \quad (7)$$

In the numerical calculations, the relative energy levels E_{1s^2}, E_{2s2p}, E_{1s}, and E_{1s2s} are 0.0, 60.149, 24.587, and 20.616 eV, respectively; the decay width $\Gamma = 0.038$ eV or its decay lifetime $1/\Gamma \approx 17$ fs [6]. Attosecond pulses with pulse duration $\tau = 0.5$ fs, much shorter than the decay lifetime of the resonance, are employed. Although the transition dipole d_{13} depends on the electron energy ε, it is a good approximation to suppose that the transition dipole is constant around the peak-electron energy [38–40], and the constant ratio between the transition dipoles $d_{13}/d_{12} = -7.6$ [6] is supposed and employed. The weak pump pulse ($\omega_1 = 60.149$ eV) is chosen so that the Rabi frequencies $\Omega_{12} = 0.0001$ a.u. or $\Omega_{13} = -0.0076$ a.u.; the control pulse ($\omega_2 = 39.533$ eV) with pulse area less than 2π will be employed.

III. RESULTS AND DISCUSSIONS

In Eq. (6), the non-Hermitian elements $D_{13}(t_1,t)$ and V correspond to the two different pathways into the ionic state $He^+(1s)$ by direct photoionization and resonance decay, respectively. Bearing in mind that the pump pulse is weak, we can approximately split $a_{1s\varepsilon p}(\varepsilon,t)$ into two parts from the bound and continuum pathways within the first order of time-dependent perturbation theory as

$$a_{1s\varepsilon p}(\varepsilon,t) = a_{1s^2\to 2s2p\to 1s\varepsilon p}(\varepsilon,t) + a_{1s^2\to 1s\varepsilon p}(\varepsilon,t). \quad (8)$$

The bound and continuum pathways interfere and result in the line profiles in the electron spectra [5–7,30,47]. The corresponding equations of motion and solutions for $a_{1s^2\to 2s2p\to 1s\varepsilon p}(\varepsilon,t)$ and $a_{1s^2\to 1s\varepsilon p}(\varepsilon,t)$ are listed in the appendix, and we have

$$\begin{aligned} &a_{1s^2\to 2s2p\to 1s\varepsilon p}(\varepsilon,t) \\ &\quad \overset{t_1<t_2<t\to\infty}{\approx} -V\sin\frac{S_1}{2}\frac{1+\left(\cos\frac{S_2}{2}-1\right)e^{-\frac{\Gamma}{2}\Delta t_{21}+i\Delta\varepsilon\Delta t_{21}}}{\frac{\Gamma}{2}-i\Delta\varepsilon} \\ &\qquad \times e^{-i\Delta\varepsilon(t-t_1)} \\ &a_{1s^2\to 1s\varepsilon p}(\varepsilon,t) \\ &\quad \overset{t\gg t_1}{\approx} -i\frac{\Omega_{13}}{2}\sqrt{\pi}\frac{e^{-\frac{\Delta\varepsilon^2\tau^2}{16\ln 2}}}{\sqrt{4\ln 2}}\tau e^{-i\Delta\varepsilon(t-t_1)}. \end{aligned} \quad (9)$$

where $S_1 = \sqrt{\frac{\pi}{4\ln 2}}\tau\Omega_{12}$ and $S_2 = \sqrt{\frac{\pi}{4\ln 2}}\tau\Omega_{24}$ are the pulse areas (the time-integrated intensity profile) for the pump and control pulses respectively, $\Delta t_{21} = t_2 - t_1$ and $\Delta\varepsilon = E_{1s} + \varepsilon - \omega_1$. Note that Eq. (9) is achieved by reasonably ignoring the resonance decay during the attosecond pulses.

For the general study of resonances with only the pump pulse, Eq. (9) can reduce into

$$\begin{aligned} a_{1s^2\to 2s2p\to 1s\varepsilon p}(\varepsilon,t) &\overset{t_1<t\to\infty}{\approx} -V\sin\frac{S_1}{2}\frac{e^{-i\Delta\varepsilon(t-t_1)}}{\frac{\Gamma}{2}-i\Delta\varepsilon} \\ a_{1s^2\to 1s\varepsilon p}(\varepsilon,t) &\overset{t\gg t_1}{\approx} -i\frac{\Omega_{13}}{2}\sqrt{\pi}\frac{e^{-\frac{\Delta\varepsilon^2\tau^2}{16\ln 2}}}{\sqrt{4\ln 2}}\tau e^{-i\Delta\varepsilon(t-t_1)}, \end{aligned} \quad (10)$$

which tells a lot about the line profiles: (1) The line profile of the bound pathway is proportional to the Lorenz profile $\frac{1}{1+(\frac{\Delta\varepsilon}{\Gamma/2})^2}$ and only depends on the decay width Γ, and the full-width half-maxima of the line profile is exactly the decay

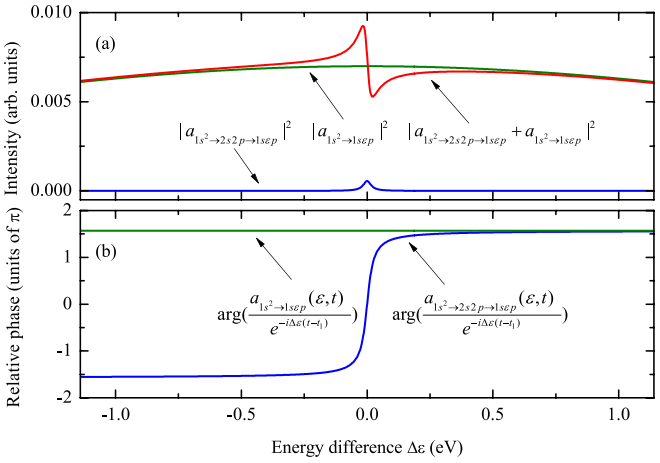

FIG. 2. Evaluations of Eq. (10) based on the parameters [below Eq. (7)] presented in the last section for resonance He($2s2p$, $^1P^o$). Panel (a) shows the absolute squares for the bound pathway $a_{1s^2\to 2s2p\to 1s\varepsilon p}$, the continuum pathway $a_{1s^2\to 1s\varepsilon p}$, and the total continuum wave packet $a_{1s\varepsilon p}$; panel (b) shows the relative phase or argument without the phase term $e^{-i\Delta\varepsilon(t-t_1)}$ for both the bound pathway and continuum pathway.

width Γ [see Fig. 2(a)]. (2) The line profile of the continuum pathway is proportional to the Gaussian profile $e^{-\frac{\Delta\varepsilon^2\tau^2}{8\ln 2}}$ and depends on the pulse duration [see Fig. 2(a)]. Note that the profile should be also modulated by the transition dipole Ω_{13}^2; however, Ω_{13}^2 can be considered as quasiconstant around the energy region of $\Delta\varepsilon$ and is not discussed here. In the limit of the long pulse with monochromatic light, $\Delta\varepsilon\to 0$ and $e^{-\frac{\Delta\varepsilon^2\tau^2}{8\ln 2}}\to 1$, the line profile can only be achieved by scanning the frequencies of the monochromatic light pulses and is quasiconstant. While in the limit of an ultrashort attosecond pulse with broad bandwidth, $\tau\to 0$ and $e^{-\frac{\Delta\varepsilon^2\tau^2}{8\ln 2}}\to 1$, the line profile is also quasiconstant around the energy region of $\Delta\varepsilon$. Actually, before the advent of the attosecond pulses, the line profiles of photoionization could only be studied by scanning the frequencies of the long pulses (e.g., synchrotron radiation); now, ultrashort attosecond pulse with broad bandwidth can interact with the system simultaneously by a bunch of different frequencies and the efficiencies are almost constant around the energy region of $\Delta\varepsilon$. (3) After throwing away the same phase term $e^{-i\Delta\varepsilon(t-t_1)}$ for the bound and continuum pathways, the continuum pathway does not change the phase around the whole energy region of $\Delta\varepsilon$, while the bound pathway changes the phase by almost π when $\Delta\varepsilon$ changes from the negative-energy region into the positive-energy region (the energy region of $\Delta\varepsilon$ is much broader than Γ) [see Fig. 2(b)]. Furthermore, supposing d_{12} and d_{13} are the signed scalars with the same sign and supposing that both transition dipoles are parallel (or antiparallel) to the induced field or d_{12}/d_{13} is positive, the bound pathway is almost out of phase and in phase with the continuum pathway in the negative- and positive-energy regions of $\Delta\varepsilon$, respectively, and vice versa. It is obvious that such kind of phasing in the negative- and positive-energy regions between the bound and continuum pathways will result in the enhancement and suppression of the cross sections in the negative- or positive-energy regions, and the electron spectra exhibit the famous asymmetric Fano profile. When d_{12} and d_{13} are the signed scalars with the same (or opposite) signs, the Fano factor $q\approx\frac{1}{\pi V}\frac{d_{12}}{d_{13}}$ [5–7] will be positive (or negative), and the electron spectra will exhibit the dip-peak (or peak-dip) line profiles with the increasing of the electron energy. (4) When only the bound pathway plays important role, or $d_{12}/d_{13}\gg 1$ and $|q|\gg 1$, such as in the case of the Auger state, the electron spectra will exhibit a peak close to the Lorenz profile. Note that when ultrashort and strong pump pulses are employed, other pathways will also play important roles, and the Auger electron spectra would be totally changed [39,48,49]. (5) Actually this model can not well describe the case with the continuum pathway only playing important role or $|d_{12}/d_{13}|\to 1$ and $|q|\to 0$, when the electron spectra will exhibit a inverse window [5–7]. In such a case, bound state $|2s2p\rangle$ does not dominate the dressed bound state any more and should be replaced by the dressed bound state, which, however, has the formal expression of the principal part of an integration and cannot be explicitly expressed [5–7,30]. Note that we will not study such cases in this work, and the above comments of Eq. (10) with only the pump pulse is significant to fully understand the buildup process of the profiles of the electron spectra.

In the present study with the attosecond pump-control scheme, the manipulation of the wave-packet dynamics of the resonance is performed with the help of a time-delayed strong control pulse with pulse area $S_2=\sqrt{\frac{\pi}{4\ln 2}}\tau\Omega_{24}$. Figure 3 shows the time-delayed photoelectron spectra for the pulses with $S_2=0.75\pi$ and $S_2=1.25\pi$, the typical cases with pulse area less than π and 2π, respectively. Note that the results are numerically solved from Eqs. (4)–(7) by giving a specific free electron energy ε and time delay $\Delta t_{21}=t_2-t_1$, which is almost the same as the analytic results of Eqs. (8) and (9) except in the time domain where two pulses largely overlap each other. As the figures show, the dynamic evolutions of the time delayed spectra are totally different for the two typical cases in the region with scaled energy $(\varepsilon-\varepsilon_0)/\Gamma\sim 0$ and $\Delta t_{21}<\sim 30$ fs.

In the case with a sub-π-control pulse [$S_2=0.75\pi$; see Fig. 3(a)], the time-delayed spectra is clearly partitioned into two regions ($\Delta t_{21}<\sim 4\tau$ and $\Delta t_{21}>\sim 4\tau$). In the region of $\Delta t_{21}<\sim 4\tau$, the pump and control pulses to some extent overlap each other, so it can be called the overlap region. In the overlap region as shown in Fig. 3(a), it is interesting to notice that the electron spectral line profiles only reduce the degrees of asymmetries compared to the ones without the control pulse. It indicates the pump and control pulses do not interact with each other too much in this overlap region with the a sub-π-control pulse, and the control pulse mainly plays the role of transferring the wave packet from the resonance (state $|2s2p\rangle$) to the control state (state $|1s2s\rangle$) and reducing the wave-packet dynamics of the resonance. In the region of $\Delta t_{21}>\sim 4\tau$, the control pulse is far behind the pump pulse and they do not overlap each other; the effects of the attosecond control pulse can be well analyzed by Eq. (9) and this can be called the analysis region. In the analysis region as shown in Fig. 3(a), the electron spectra are characterized by the modulation structures and close to asymmetry profiles without the control pulse. These features can be easily understood with the help of Eq. (9). The phase term $e^{i\Delta\varepsilon\Delta t_{21}}$ results in the

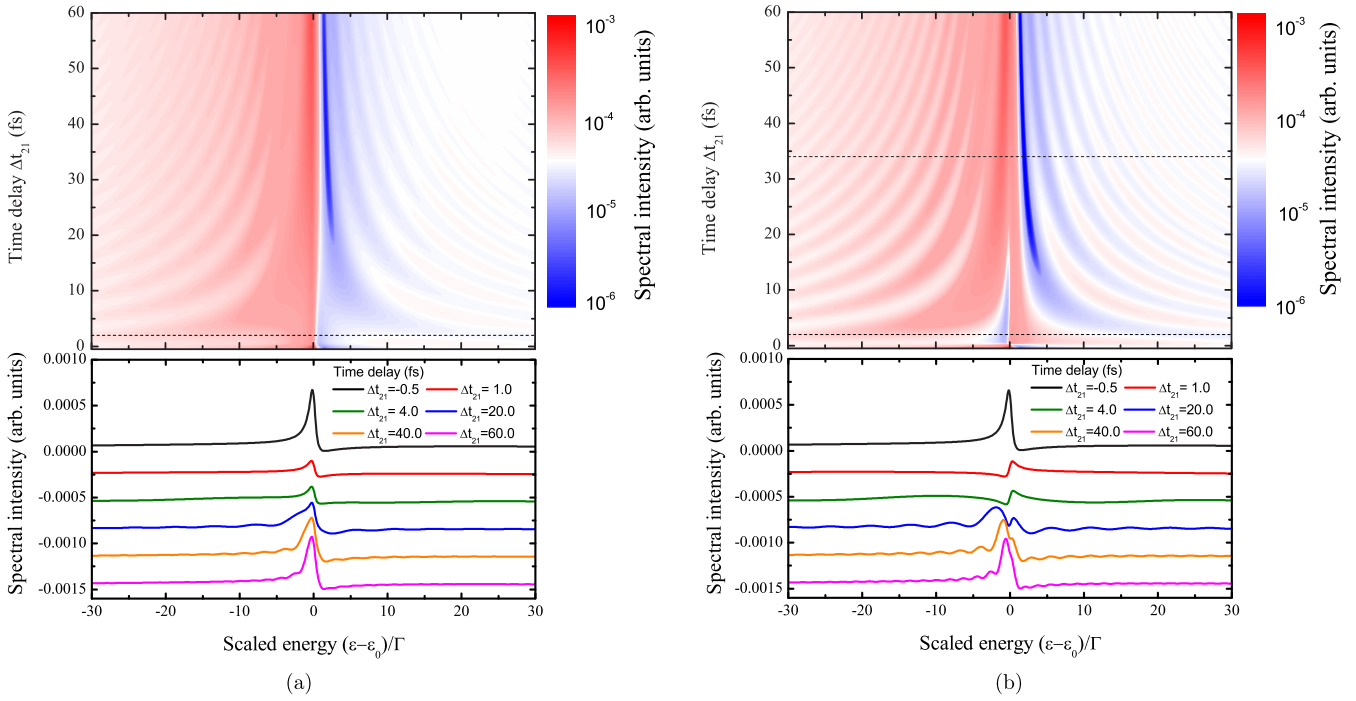

FIG. 3. Time-delayed photoelectron spectra $|a_{1s\varepsilon p}|^2$ with attosecond control pulses of pulse area $S_2 = 0.75\pi$ (a) and 1.25π (b), $\varepsilon_0 = E_{1s} - \omega_1 = 35.562$ eV and $\Gamma = 0.038$ eV. The upper panels are the contour plots of the spectral intensity with respect to the time delay Δt_{21} and scaled energy $(\varepsilon - \varepsilon_0)/\Gamma$; the lower panels are the snapshots of the spectral intensity for selected time delays. The lower and upper horizontal dashed lines in the upper panels correspond to time delay $\Delta t_{21} = 4\tau$ (2 fs) and $2/\Gamma$ (34 fs), respectively, which can be approximately considered as the division of different spectral regions. To better differentiate the curves in the lower panels, the curves for $\Delta t_{21} = 1.0$, 4.0, 20.0, 40.0, and 60.0 fs have been shifted down by 0.0003, 0.0006, 0.0009, 0.0012, and 0.0015 arbitrary units, respectively.

modulation structures in the spectra. With the increasing of the time delay, the modulation turns more apparent; however, the fast decay term $e^{-\frac{\Gamma}{2}\Delta t_{21}}$ (proportional to the remaining wave packet of the resonance when the control pulse is on) reduces its depths. The term $1 + (\cos\frac{S_2}{2} - 1)e^{-\frac{\Gamma}{2}\Delta t_{21} + i\Delta\varepsilon\Delta t_{21}}$ shows the intensity of the wave packet of the resonance after the control pulse. Obviously when the time delay is very big, the remaining wave packet of the resonance, proportional to the fast decay term $e^{-\frac{\Gamma}{2}\Delta t_{21}}$, that can be manipulated by the control pulse is negligible, and the electron spectra return into the ones without the control pulse. In most cases with a short time delay, the sub-π-control pulse turns $\cos\frac{S_2}{2} - 1 < 0$ and the phase of $1 + (\cos\frac{S_2}{2} - 1)e^{-\frac{\Gamma}{2}\Delta t_{21} + i\Delta\varepsilon\Delta t_{21}}$ is almost around zero, which equals the reduction of the transition matrix d_{12} and the Fano factor $|q \approx \frac{1}{\pi V}\frac{d_{12}}{d_{13}}|$ (the sign of q does not change), and therefore the asymmetric profiles of the electron spectra of the resonance do not change but only become reduced.

In the case with a sub-2π-control pulse [$S_2 = 1.25\pi$; see Fig. 3(b)], the time-delayed spectra can also be roughly partitioned into the overlap region ($\Delta t_{21} <\sim 4\tau$) and analysis region ($\Delta t_{21} >\sim 4\tau$); however, as shown in Fig. 3(b), it would be more appropriate to partition the analysis region into a reverse region ($\sim 4\tau < \Delta t_{21} \lesssim 2/\Gamma$) and the analysis region ($\Delta t_{21} \gtrsim 2/\Gamma$), since the line profiles of the spectra in the reverse region experience asymmetric changes from that of Fig. 3(a). In the overlap region, the sub-2π-control pulse is strong enough to cycle the wave packet of the resonance back to the resonance through the control state with the phase changed by π, and provides a new pathway to interfere with the wave packet of the resonance by the pump pulse. The strong interaction results in the changes of the sign of the Fano factor q and the electron spectra totally reverse their line profiles from the peak-dip asymmetry into the dip-peak asymmetry. In the rest region, the electron spectra are characterized by the modulation structures from the phase term $e^{i\Delta\varepsilon\Delta t_{21}}$, while the spectra gradually reverse back the line profiles from the dip-peak asymmetry into peak-dip asymmetry with the increasing of time delay from the reverse region into the analysis region. The variations of the electron spectra in both reverse and analysis regions can be analyzed by Eq. (9); the differences come from the results of the fast decay term $e^{-\frac{\Gamma}{2}\Delta t_{21}}$, characterizing the remaining wave packet of the resonance that can be revered by the attosecond sub-2π-control pulse. In the reverse region ($\sim 4\tau < \Delta t_{21} \lesssim 2/\Gamma$) with $e^{-\frac{\Gamma}{2}\Delta t_{21}} > e^{-1}$, the accumulated decays from the reversed wave packet with phase changed by π by the control pulse dominate contributions to the electron spectra and the electron spectra exhibit the dip-peak profiles from the π-phase-changed wave packet after the control pulse; while in the analysis region ($\Delta t_{21} \gtrsim 2/\Gamma$) with $e^{-\frac{\Gamma}{2}\Delta t_{21}} < e^{-1}$, where there is not much remaining wave packet of the resonance that can be reversed by the control pulse, the electron spectra would keep the peak-dip profiles and gradually return into the case without the control pulse with the increase of time delays. Note that the profiles of the time-delayed spectra exhibit different features in different regions and change gradually through different regions with respect to the time delay; the exact division for the regions should be meaningless. However, the different features of

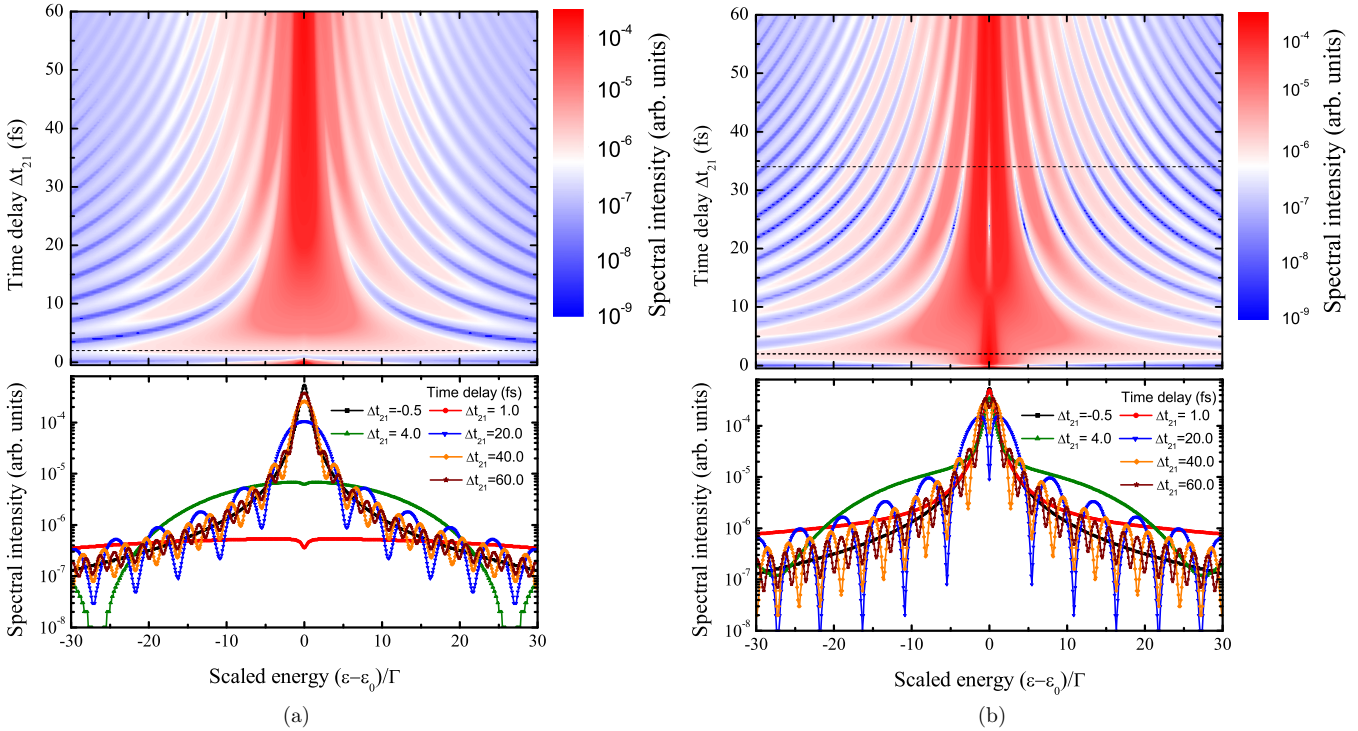

FIG. 4. Similar to Fig. 3, but for the time-delayed module squares of the bound pathway $|a_{1s^2\to 2s2p\to 1s\varepsilon p}|^2$ with attosecond control pulses of pulse area $S_2 = \pi$ (a) and 2π (b), and the curves in the lower panels are not shifted.

the spectra in different regions come from different physical origins, the division of the spectra should be significant, and the present divisions around 4τ and $2/\Gamma$ should be reasonable. The case in which the control pulse comes much earlier than the pump pulse (no overlap between the pulses) is not necessarily or explicitly presented and discussed. In such a case, the control pulse plays no role, since the resonance has not yet been created by the pump pulse while the control pulse has gone, and such a case should be the same as the case with only the pump pulse (no control pulse).

In the two limited cases of π- and 2π-control pulses, the π-control pulse can totally empty the population of the resonance and freeze its wave-packet dynamics, the snapshot of the wave packet of the resonance is imprinted in the electron spectra, and the attosecond π-control pulse acts as a scissor and breaks down the wave-packet dynamics instantly. The 2π-control pulse can change the phase of all the remaining wave packets of the resonance by π, resulting in the greatest changes of the wave-packet dynamics and the line profiles of the electron spectra. The present pump-control scheme directly interrupts the bound pathway to manipulate the electron spectra, and resonances with the dominated channel of the bound pathway, such as Auger states, should be more efficiently performed and observed. Figure 4 shows the time-delayed module squares of only the bound pathway $|a_{1s^2\to 2s2p\to 1s\varepsilon p}|^2$, to approximately simulate the electron spectra of Auger states, in the cases of π- and 2π-control pulses. As revealed in the figure, despite the very clear modulation structures from the phase term $e^{i\Delta\varepsilon\Delta t_{21}}$, the changes of the amplitude with respect to the time decay Δt_{21} around $\Delta\varepsilon = 0$ are also very significant, and the spectra exhibit clear dips around $\Delta\varepsilon = 0$ in a broad range in the region $\sim 4\tau < \Delta t_{21} \lesssim 2/\Gamma$ for $S_2 = 2\pi$. Bearing in mind that the advent of multicolor strong attosecond x ray is feasible at present FELs [31–37] and the Auger electron spectra is clean with negligible background, the present scheme could be first implemented for Auger states.

IV. CONCLUSIONS

In conclusion, we propose an attosecond XUV or x-ray pump-control scheme for the manipulation of electron spectral line profiles of Fano and Auger resonances. All the dynamic features of the electron spectra are fully understood with the help of analytic theory, which is also presented based on the time-dependent perturbation theory. In the present pump-control scheme, an weak pump resonantly excites the ground state of an atom and creates the resonance, and a second strong attosecond control pulse resonantly couples the resonance to an valance excited state at different time delays (Δt_{21}). Resonance with lifetime (Γ) much longer than the pulse duration (τ) is studied. It is found that the dynamic variations of the electron spectra can be partitioned into overlap region ($\Delta t_{21} \lesssim 4\tau$) and analysis region ($\Delta t_{21} \gtrsim 4\tau$) in the case with a sub-π-control pulse; and overlap region ($\Delta t_{21} \lesssim 4\tau$), reverse region ($\sim 4\tau < \Delta t_{21} \lesssim 2/\Gamma$), and analysis region ($\Delta t_{21} \gtrsim 2/\Gamma$) in the case with a sub-2π-control pulse. In the case with a sub-π-control pulse, the electron spectral line profiles do not change too much and only the degrees of asymmetries are reduced in the overlap region. In the analysis region, the main profiles

of the electron spectra are maintained but with modulation structures. In the case with a sub-2π-control pulse, the electron spectral line profiles totally reverse the asymmetries in the overlap region, while in the reverse region, the electron spectra keep the reversed asymmetries but with modulation structures. The electron spectra pertain to the modulation structures in the analysis region but with the main profiles reversed back. Although the helium resonance $|2s2p,\,^1P\rangle$ (strictly speaking, $|2s2p,\,^1P\rangle$ should be the Feshbach resonance of He^+) is studied as an example, the conclusion of this work is of broad interest and can be extended to other resonance and other systems.

ACKNOWLEDGMENTS

Grants from the National Basic Research Program of China (No. 2013CB922200), Shaanxi Normal University, the Organization Department of CCCPC, NSFC (No. 11604197), and the Science Challenge Program of China (No. TZ2016005) are acknowledged.

APPENDIX

This part presents the analytical solutions for Eqs. (4)–(6) with conditions. With the weak pump pulse and in the first order of time-dependent perturbation theory, the wave packet of the ground state can be well supposed as $a_{1s^2}(t)\approx 1$, and bearing in mind that the non-Hermitian elements $D_{13}(t_1,t)$ and V in Eq. (6) correspond to the two different pathways into the ionic state by direct photoionization and resonance decay, respectively, Eqs. (4)–(6) can be approximately split into the following two sets with the resonant pulses as

$$\begin{bmatrix} 0 & 0 \\ \frac{\Omega_{13}}{2}g(t_1,t) & \Delta\varepsilon \end{bmatrix}\begin{bmatrix} a_{1s^2}(t) \\ a_{1s^2\to 1s\varepsilon p}(\varepsilon,t) \end{bmatrix} = i\begin{bmatrix} \dot{a}_{1s^2}(t) \\ \dot{a}_{1s^2\to 1s\varepsilon p}(\varepsilon,t) \end{bmatrix} \tag{A1}$$

and

$$\begin{bmatrix} 0 & \frac{\Omega_{12}}{2}g(t_1,t) & 0 & 0 \\ \frac{\Omega_{12}}{2}g(t_1,t) & -\frac{i}{2}\Gamma & 0 & \frac{\Omega_{24}}{2}g(t_2,t) \\ 0 & V & \Delta\varepsilon & 0 \\ 0 & \frac{\Omega_{24}}{2}g(t_2,t) & 0 & 0 \end{bmatrix}\begin{bmatrix} a_{1s^2}(t) \\ a_{2s2p}(t) \\ a_{1s^2\to 2s2p\to 1s\varepsilon p}(\varepsilon,t) \\ a_{1s2s}(t) \end{bmatrix} = i\begin{bmatrix} \dot{a}_{1s^2}(t) \\ \dot{a}_{2s2p}(t) \\ \dot{a}_{1s^2\to 2s2p\to 1s\varepsilon p}(\varepsilon,t) \\ \dot{a}_{1s2s}(t) \end{bmatrix}, \tag{A2}$$

where $\Delta\varepsilon = E_{1s}+\varepsilon-\omega_1$, $g(t_i,t) = e^{-4\ln 2\frac{(t-t_i)^2}{\tau^2}}$, $a_{1s\varepsilon p}(\varepsilon,t) = a_{1s^2\to 2s2p\to 1s\varepsilon p}(\varepsilon,t)+a_{1s^2\to 1s\varepsilon p}(\varepsilon,t)$, and $a_{1s^2}\approx 1$. Note that in the numerical calculation, the equations are propagated from time zero, and the pulse center is set far from time zero, or $t_i \gg 0$, and we keep these conditions here. $a_{1s^2\to 1s\varepsilon p}(\varepsilon,t)$ can be solved from Eq. (A1) for time far from the pump pulse or $t \gg t_1$ as

$$a_{1s^2\to 1s\varepsilon p}(\varepsilon,t) \overset{t\gg t_1}{\approx} -ie^{-i\Delta\varepsilon t}\int_0^t \frac{\Omega_{13}}{2}g(t_1,t)e^{i\Delta\varepsilon t}dt = -i\frac{\Omega_{13}}{2}\sqrt{\pi}\frac{e^{-\frac{\Delta\varepsilon^2\tau^2}{16\ln 2}}}{\sqrt{4\ln 2}}\tau e^{-i\Delta\varepsilon(t-t_1)}. \tag{A3}$$

The solutions of Eq. (A2) can be imposed with some conditions. We consider the case of the attosecond control pulse far from the pump pulse or $t_2 \gg t_1$, and bearing in mind that the pulses are much shorter than the decay lifetime or $\tau \ll 1/\Gamma$, the resonant excitation to $a_{2s2p}(t)$ and the spontaneous decay to $a_{1s^2\to 2s2p\to 1s\varepsilon p}(\varepsilon,t)$ can be well approximated into two independent steps: First, $a_{2s2p}(t)$ is excited by the pulses by ignoring the decay during the pulse, and then the decay to $a_{1s^2\to 2s2p\to 1s\varepsilon p}(\varepsilon,t)$ takes place by shifting the staring time to the pulse center. With these assumptions, $a_{2s2p}(t)$ can be well solved as

$$a_{2s2p}(t) \overset{t>t_1}{\approx} \begin{cases} -i\sin\frac{S_1}{2}e^{-\frac{\Gamma}{2}(t-t_1)}, t < t_2 \\ -i\cos\frac{S_2}{2}\sin\frac{S_1}{2}e^{-\frac{\Gamma}{2}(t-t_1)}, t \geqslant t_2 \end{cases}, \tag{A4}$$

where $S_1 = \sqrt{\frac{\pi}{4\ln 2}}\tau\Omega_{12}$ and $S_2 = \sqrt{\frac{\pi}{4\ln 2}}\tau\Omega_{24}$ are the pulse areas for the pump and control pulse respectively. The terms of $-i\sin\frac{S_1}{2}$ and $\cos\frac{S_2}{2}$ are related to the excitations by the attosecond pump pulse and probe pulse by ignoring the decay during these pulses, respectively, and $e^{-\frac{\Gamma}{2}(t-t_1)}$ corresponds to the relatively long resonance decay part. Finally, $a_{1s^2\to 2s2p\to 1s\varepsilon p}(\varepsilon,t)$ can be achieved as

$$\begin{aligned} a_{1s^2\to 2s2p\to 1s\varepsilon p}(\varepsilon,t) &\overset{t_1<t_2<t}{\approx} -iVe^{-i\Delta\varepsilon(t-t_1)}\int_{t_i}^t a_{2s2p}(t')e^{-\frac{\Gamma}{2}(t'-t_1)}e^{i\Delta\varepsilon(t'-t_1)}dt' \\ &\overset{t_1<t_2<t}{\approx} -V\sin\frac{S_1}{2}\frac{1+\left(\cos\frac{S_2}{2}-1\right)e^{-\frac{\Gamma}{2}\Delta t_{21}+\Delta\varepsilon\Delta t_{21}}-e^{-\frac{\Gamma}{2}(t-t_1)+i\Delta\varepsilon(t-t_1)}}{\frac{\Gamma}{2}-i\Delta\varepsilon}e^{-i\Delta\varepsilon(t-t_1)} \\ &\overset{t_1<t_2<t\to\infty}{\approx} -V\sin\frac{S_1}{2}\frac{1+\left(\cos\frac{S_2}{2}-1\right)e^{-\frac{\Gamma}{2}\Delta t_{21}+i\Delta\varepsilon\Delta t_{21}}}{\frac{\Gamma}{2}-i\Delta\varepsilon}e^{-i\Delta\varepsilon(t-t_1)}, \end{aligned} \tag{A5}$$

where $\Delta t_{21} = t_2 - t_1$. For the case without the control pulse, Eq. (A5) can reduce into

$$a_{1s^2\to 2s2p\to 1s\varepsilon p}(\varepsilon,t) \overset{t_1<t\to\infty}{\approx} -V \sin\frac{S_1}{2}\frac{e^{-i\Delta\varepsilon(t-t_1)}}{\frac{\Gamma}{2}-i\Delta\varepsilon}. \tag{A6}$$

[1] C. J. Joachain, *Quantum Collision Theory* (North-Holland, Amsterdam, 1975).

[2] J. R. Taylor, *Scattering Theory: The Quantum Theory of Nonrelativistic Collisions* (Courier Corporation, New York, 2006).

[3] P. G. Burke, *R-Matrix Theory of Atomic Collisions: Application to Atomic, Molecular, and Optical Processes* (Springer Science & Business Media, Berlin, 2011).

[4] H. S. Friedrich, *Theoretical Atomic Physics* (Springer Science & Business Media, Berlin, 2005).

[5] U. Fano, Effects of configuration interaction on intensities and phase shifts, Phys. Rev. **124**, 1866 (1961).

[6] U. Fano and J. W. Cooper, Line profiles in the far-uv absorption spectra of the rare gases, Phys. Rev. **137**, A1364 (1965).

[7] U. Fano and J. W. Cooper, Spectral distribution of atomic oscillator strengths, Rev. Mod. Phys. **40**, 441 (1968).

[8] P. G. Burke and W. D. Robb, The r-matrix theory of atomic processes, Adv. At. Mol. Phys. **11**, 143 (1976).

[9] S. B. Zhang, J. G. Wang, and R. K. Janev, Crossover of Feshbach Resonances to Shape-Type Resonances in Electron-Hydrogen Atom Excitation with a Screened Coulomb Interaction, Phys. Rev. Lett. **104**, 023203 (2010).

[10] S. B. Zhang, J. G. Wang, R. K. Janev, and X. J. Chen, Electron collisions with the bh2 radical using the r-matrix method, Phys. Rev. A **82**, 062711 (2010).

[11] S. B. Zhang and D. L. Yeager, Complex-scaled multireference configuration-interaction method to study Be and Be-like cations' (B, C, N, O, Mg) Auger resonances $1s2s^22p^{1,3}p^o$, Phys. Rev. A **85**, 032515 (2012).

[12] Y. Wu, X. H. Lin, B. Yan, J. G. Wang, and R. K. Janev, Theoretical investigation of electron transfer and detachment processes in low energy $H^- + Li$ and $Li^- + H$ collisions, J. Phys. B **49**, 035203 (2016).

[13] A. F. White, E. Epifanovsky, C. W. McCurdy, and M. Head-Gordon, Second order Möller-Plesset and coupled cluster singles and doubles methods with complex basis functions for resonances in electron-molecule scattering, J. Chem. Phys. **146**, 234107 (2017).

[14] C. Ott, A. Kaldun, P. Raith, K. Meyer, M. Laux, J. Evers, C. H. Keitel, C. H. Greene, and T. Pfeifer, Lorentz meets Fano in spectral line shapes: A universal phase and its laser control, Science **340**, 716 (2013).

[15] A. Kaldun, C. Ott, A. Blättermann, M. Laux, K. Meyer, T. Ding, A. Fischer, and T. Pfeifer, Extracting Phase and Amplitude Modifications of Laser-Coupled Fano Resonances, Phys. Rev. Lett. **112**, 103001 (2014).

[16] M. Chini, K. Zhao, and Z. Chang, The generation, characterization, and applications of broadband isolated attosecond pulses, Nat. Photon. **8**, 178 (2014).

[17] B. Bernhardt, A. R. Beck, X. Li, E. R. Warrick, M. J. Bell, D. J. Haxton, C. W. McCurdy, D. M. Neumark, and S. R. Leone, High-spectral-resolution attosecond absorption spectroscopy of autoionization in xenon, Phys. Rev. A **89**, 023408 (2014).

[18] K. P. Heeg, C. Ott, D. Schumacher, H.-C. Wille, R. Röhlsberger, T. Pfeifer, and J. Evers, Interferometric Phase Detection at X-Ray Energies Via Fano Resonance Control, Phys. Rev. Lett. **114**, 207401 (2015).

[19] M. Kotur, D. Guénot, Á Jiménez-Galán, D. Kroon, E. W. Larsen, M. Louisy, S. Bengtsson, M. Miranda, J. Mauritsson, and C. L. Arnold, Spectral phase measurement of a Fano resonance using tunable attosecond pulses, Nat. Commun. **7**, 10566 (2016).

[20] A. Kaldun, A. Blättermann, V. Stooß, S. Donsa, H. Wei, R. Pazourek, S. Nagele, C. Ott, C. D. Lin, J. Burgdörfer *et al.*, Observing the ultrafast buildup of a Fano resonance in the time domain, Science **354**, 738 (2016).

[21] V. Gruson, L. Barreau, Á. Jiménez-Galan, F. Risoud, J. Caillat, A. Maquet, B. Carré, F. Lepetit, J.-F. Hergott, and T. Ruchon, Attosecond dynamics through a Fano resonance: Monitoring the birth of a photoelectron, Science **354**, 734 (2016).

[22] A. Zielinski, V. P. Majety, S. Nagele, R. Pazourek, J. Burgdörfer, and A. Scrinzi, Anomalous Fano Profiles in External Fields, Phys. Rev. Lett. **115**, 243001 (2015).

[23] Z. Q. Yang, D. F. Ye, T. Ding, T. Pfeifer, and L. B. Fu, Attosecond xuv absorption spectroscopy of doubly excited states in helium atoms dressed by a time-delayed femtosecond infrared laser, Phys. Rev. A **91**, 013414 (2015).

[24] E. Heinrich-Josties, S. Pabst, and R. Santra, Controlling the $2p$ hole alignment in neon via the $2s$-$3p$ Fano resonance, Phys. Rev. A **89**, 043415 (2014).

[25] C.-T. Liao, X. Li, D. J. Haxton, T. N. Rescigno, R. R. Lucchese, C. W. McCurdy, and A. Sandhu, Probing autoionizing states of molecular oxygen with xuv transient absorption: Electronic-symmetry-dependent line shapes and laser-induced modifications, Phys. Rev. A **95**, 043427 (2017).

[26] M. J. Akram, F. Ghafoor, M. M. Khan, and F. Saif, Control of Fano resonances and slow light using Bose-Einstein condensates in a nanocavity, Phys. Rev. A **95**, 023810 (2017).

[27] W.-C. Chu and C. D. Lin, Absorption and emission of single attosecond light pulses in an autoionizing gaseous medium dressed by a time-delayed control field, Phys. Rev. A **87**, 013415 (2013).

[28] Y. Kobayashi, H. Timmers, M. Sabbar, S. R. Leone, and D. M. Neumark, Attosecond transient-absorption dynamics of xenon core-excited states in a strong driving field, Phys. Rev. A **95**, 031401 (2017).

[29] S. B. Zhang, V. Kimberg, and N. Rohringer, Nonlinear resonant Auger spectroscopy in Co using an x-ray pump-control scheme, Phys. Rev. A **94**, 063413 (2016).

[30] P. L. Knight, M. A. Lauder, and B. J. Dalton, Laser-induced continuum structure, Phys. Rep. **190**, 1 (1990).

[31] A. A. Lutman, R. Coffee, Y. Ding, Z. Huang, J. Krzywinski, T. Maxwell, M. Messerschmidt, and H. D. Nuhn, Experimen-

tal Demonstration of Femtosecond Two-Color X-Ray Free-Electron Lasers, Phys. Rev. Lett. **110**, 134801 (2013).

[32] E. Allaria, F. Bencivenga, R. Borghes, F. Capotondi, D. Castronovo, P. Charalambous, P. Cinquegrana, M. B. Danailov, G. De Ninno, A. Demidovich *et al.*, Two-colour pump-probe experiments with a twin-pulse-seed extreme ultraviolet free-electron laser, Nat. Commun. **4**, 2476 (2013).

[33] A. Marinelli, D. Ratner, A. A. Lutman, J. Turner, J. Welch, F. J. Decker, H. Loos, C. Behrens, S. Gilevich, A. A. Miahnahri *et al.*, High-intensity double-pulse x-ray free-electron laser, Nat. Commun. **6**, 6369 (2015).

[34] W. Helml, A. R. Maier, W. Schweinberger, I. Grguraš, P. Radcliffe, G. Doumy, C. Roedig, J. Gagnon, M. Messerschmidt, S. Schorb *et al.*, Measuring the temporal structure of few-femtosecond free-electron laser x-ray pulses directly in the time domain, Nat. Photon. **8**, 950 (2014).

[35] N. Hartmann, W. Helml, A. Galler, M. R. Bionta, J. Grünert, S. L. Molodtsov, K. R. Ferguson, S. Schorb, M. L. Swiggers, S. Carron *et al.*, Sub-femtosecond precision measurement of relative x-ray arrival time for free-electron lasers, Nat. Photon. **8**, 706 (2014).

[36] K. C. Prince, E. Allaria, C. Callegari, R. Cucini, G. De Ninno, S. Di Mitri, B. Diviacco, E. Ferrari, P. Finetti, D. Gauthier *et al.*, Coherent control with a short-wavelength free-electron laser, Nat. Photon. **10**, 176 (2016).

[37] N. Hartmann and J. M. Glownia, X-ray photonics: Attosecond coherent control at fels, Nat. Photon. **10**, 148 (2016).

[38] E. Pahl, H. D. Meyer, and L. S. Cederbaum, Competition between excitation and electronic decay of short-lived molecular states, Z. Phys. D **38**, 215 (1996).

[39] P. V. Demekhin, Y.-C. Chiang, and L. S. Cederbaum, Resonant Auger decay of the core-excited C^*O molecule in intense x-ray laser fields, Phys. Rev. A **84**, 033417 (2011).

[40] S. B. Zhang and N. Rohringer, Photoemission spectroscopy with high-intensity short-wavelength lasers, Phys. Rev. A **89**, 013407 (2014).

[41] S. B. Zhang and N. Rohringer, Quantum-beat Auger spectroscopy, Phys. Rev. A **92**, 043420 (2015).

[42] J. M. Lecomte, A. Kirrander, and C. Jungen, Time-dependent resonant scattering: An analytical approach, J. Chem. Phys. **139**, 164111 (2013).

[43] B. W. Shore, *Manipulating Quantum Structures Using Laser Pulses* (Cambridge University Press, New York, 2011).

[44] E. Gamaly, *Femtosecond Laser-Matter Interaction: Theory, Experiments, and Applications* (Pan Stanford, Singapore, 2011).

[45] W. Domcke, Theory of resonance and threshold effects in electron-molecule collisions: The projection-operator approach, Phys. Rep. **208**, 97 (1991).

[46] L. S. Cederbaum and W. Domcke, Local against non-local complex potential in resonant electron-molecule scattering, J. Phys. B **14**, 4665 (1981).

[47] C. D. Lin and W.-C. Chu, Controlling atomic line shapes, Science **340**, 694 (2013).

[48] A. D. Müller and P. V. Demekhin, Resonant auger decay of the $4d \rightarrow 6p$ excitation in xe driven by short intense coherent soft x-ray pulses, J. Phys. B **48**, 075602 (2015).

[49] P. V. Demekhin and L. S. Cederbaum, Resonant Auger decay of core-excited CO molecules in intense x-ray laser pulses: The $O(1s \rightarrow \Pi*)$ excitation, J. Phys. B **46**, 164008 (2013).